CDDpress

www.nature.com/cddis

ARTICLE OPEN

Systems biology-enabled targeting of NF-κB and BCL2 overcomes microenvironment-mediated BH3-mimetic resistance in DLBCL

Aimilia Vareli[1], Haripriya Vaidehi Narayanan[2], Heather Clark[1], Eleanor Jayawant[1], Hui Zhou[3], Yi Liu[3], Emma Kennedy[1], Lauren Stott[1], Fabio Simoes[1], Alexander Hoffmann[2], Andrea Pepper[1], Chris Pepper[1] and Simon Mitchell[1]✉

In Diffuse Large B-cell Lymphoma (DLBCL), elevated anti-apoptotic BCL2-family proteins (e.g., MCL1, BCL2, BCLXL) and NF-κB subunits (RelA, RelB, cRel) confer poor prognosis. Heterogeneous expression, regulatory complexity, and redundancy offsetting the inhibition of individual proteins, complicate the assignment of targeted therapy. We combined flow cytometry 'fingerprinting', immunofluorescence imaging, and computational modeling to identify therapeutic vulnerabilities in DLBCL. The combined workflow predicted selective responses to BCL2 inhibition (venetoclax) and non-canonical NF-κB inhibition (Amgen16). Within the U2932 cell line we identified distinct resistance mechanisms to BCL2 inhibition in cellular sub-populations recapitulating intratumoral heterogeneity. Co-cultures with CD40L-expressing stromal cells, mimicking the tumor microenvironment (TME), induced resistance to BCL2 and BCLXL targeting BH3-mimetics via cell-type specific upregulation of BCLXL or MCL1. Computational models, validated experimentally, showed that basal NF-κB activation determined whether CD40 activation drove BH3-mimetic resistance through upregulation of RelB and BCLXL, or cRel and MCL1. High basal NF-κB activity could be overcome by inhibiting BTK to resensitize cells to BH3-mimetics in CD40L co-culture. Importantly, non-canonical NF-κB inhibition overcame heterogeneous compensatory BCL2 upregulation, restoring sensitivity to both BCL2- and BCLXL-targeting BH3-mimetics. Combined molecular fingerprinting and computational modelling provides a strategy for the precision use of BH3-mimetics and NF-κB inhibitors in DLBCL.

Cell Death and Disease (2025)16:620 ; https://doi.org/10.1038/s41419-025-07942-0

INTRODUCTION

Diffuse large B-cell lymphoma (DLBCL), is an aggressive blood cancer [1]. First line treatment is only successful in approximately 60% of patients [2–5]. The highly heterogenous nature of the disease has challenged advancing the standard of care through one-size-fits-all approaches [6–11]. Activated B-cell (ABC) DLBCL patients bearing Nuclear Factor-κappa light chain enhancer of B cells (NF-κB) activating mutations, and Germinal Center (GC) DLBCL patients with *BCL2*-activating mutations have particularly poor prognosis [11].

NF-κB is a dimeric transcription factor composed of combinations of five proteins (RelA, RelB, cRel, p50 and p52), which are normally sequestered in the cytoplasm by a combination of four inhibitors of NF-κB (IκBα, -β, -δ, and-ε) [12, 13]. The IκB proteins have distinct affinities for different NF-κB dimers with IκBα predominantly inhibiting RelA-containing dimers and IκB-δ and -ε regulating cRel-containing dimers in a context-specific manner [14, 15]. The abundance and nuclear localization of individual NF-κB components is prognostically informative in DLBCL [16–18]. Heterogeneity in NF-κB subunits can be quantified and visualized using flow cytometry to reveal unique 'fingerprints' of NF-κB, with heterogenous levels of individual NF-κB proteins found within ABC-DLBCL [19]. Two NF-κB pathways (canonical and non-canonical) may be activated by a combination of tumor microenvironmental signaling and activating mutations in DLBCL leading to nuclear translocation of NF-κB [20]. While targeting NF-κB has shown therapeutic potential in subgroups of blood cancer patients [21–26], heterogeneity and toxicities associated with global targeting of the canonical NF-κB pathway has challenged clinical progress. The oncogenic role of NF-κB in lymphoma is largely attributed to the anti-apoptotic gene expression induced upon NF-κB activation [26, 27].

Anti-apoptotic BCL2 family proteins, including Myeloid Cell Leukemia 1 (MCL1) and B-cell Lymphoma-extra Large (BCLXL), are inhibitors of the intrinsic pathway of apoptosis [28, 29], and are often overexpressed in DLBCL as a result of gene translocation events, gene amplifications, mutations within open reading frames, and microenvironment-mediated increased NF-κB activity [30]. BCL2 is an attractive target in DLBCL, and the specific BCL2 inhibitor venetoclax is clinically used for multiple hematological

[1]Department of Clinical and Experimental Medicine, Brighton and Sussex Medical School, University of Brighton and University of Sussex, Brighton BN1 9PX, UK. [2]Signaling Systems Laboratory, Department of Microbiology, Immunology, and Molecular Genetics, and Institute for Quantitative and Computational Biosciences, University of California, Los Angeles, Los Angeles, CA, USA. [3]DeepKinase Biotechnologies, Kunshan, China. ✉email: S.A.Mitchell@bsms.ac.uk

Edited by Marco Herold

Received: 4 February 2025 Revised: 26 June 2025 Accepted: 4 August 2025
Published online: 16 August 2025

malignancies [31]. However, venetoclax has shown limited efficacy in DLBCL clinical trials [31, 32]. BCL2-family proteins (MCL1 and BCLXL) are often over expressed in DLBCL with elevated expression conferring venetoclax resistance by compensating for the sequestration of BCL2 [33, 34]. BH3-profiling, established in 2006, measured the impact of BH3-peptides on mitochondrial outer membrane permeabilization [35]. While predictive of response to BCL2 antagonism in pre-clinical studies, responses to BH3-mimetics in drug response assays can differ, and BH3-profiling has not translated into prospective assignment of therapies in clinical trials of lymphoma [36–38].

The daunting complexity of both NF-κB regulatory networks, and apoptotic signaling regulation, has motivated the use of computational systems biology models to predict responses to BH3-mimetics [39], responses to the tumor microenvironment (TME) [19, 40], and predict the impact of mutations on clinical outcome [19, 41]. Recent single-cell RNA sequencing of DLBCL patient material revealed the primary impact of the TME is through CD40 and B-cell activating factor (BAFF), which activate non-canonical NF-κB [42]. The regulation of BCLXL by non-canonical NF-κB (RelB) is established in CLL [25]. However, how heterogeneity in multiple NF-κB proteins results in anti-apoptotic protein heterogeneity in the context of the TME, and controls response to BH3-mimetics is unknown and has the potential unlock the deployment of targeted therapies such as BH3-mimetics and NF-κB inhibitors (Fig. 1).

In this study, we combined molecular fingerprinting, immunofluorescence imaging, and computational modeling to reveal how heterogeneity in NF-κB in response to TME signals shape anti-apoptotic dependencies in DLBCL. This integrated approach uncovered heterogeneous mechanisms of resistance to BH3-mimetics and demonstrated that targeting non-canonical NF-κB activation can overcome TME-mediated BH3-mimetic resistance. We also identified crosstalk between non-canonical and canonical NF-κB activity, which results in distinct induction of BC2-family proteins and enables canonical NF-κB inhibition to also resensitize these DLBCL cells in the context of TME-mediated BH3-mimetic resistance.

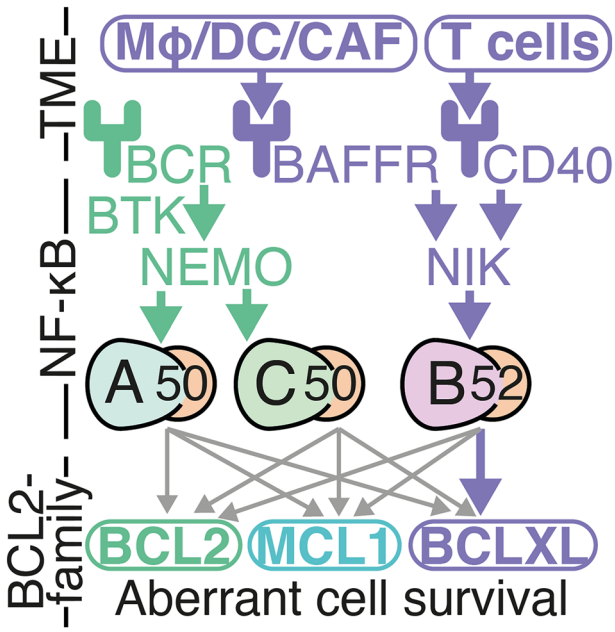

Fig. 1 Summary of existing knowledge of links between the Tumor Microenvironment (TME), NF-κB dimers, and BCL2-family proteins in lymphoma. The canonical NF-κB pathway (green) is mediated in part by B-cell receptor (BCR) signaling. BCR signaling transduces signals through Bruton's tyrosine kinase (BTK), and NF-κB essential modulator (NEMO), to primarily activate RelA- and cRel-containing NF-κB dimers. Single cell RNA sequencing has revealed that the primary impact of the TME on DLBCL cells is through the non-canonical NF-κB pathway (purple). Macrophages (Mϕ), dendritic cells (DC), and cancer associated fibroblasts (CAFS), activate non-canonical signaling through B cell-activating factor receptor (BAFFR). T cells in the TME secrete CD40 ligand. Both BAFFR and CD40 activation lead to stabilization of NF-κB-inducing kinase (NIK) and activation of RelB-containing NF-κB dimers. While RelB activity has been shown to upregulate BCLXL in chronic lymphocytic leukemia, and there are frequently reported links between NF-κB and BCL2, it is unknown which NF-κB dimers induce which BCL2-family proteins (indicated by gray arrows), and how this drives response to therapies in the context of the DLBCL TME.

METHODS

Mice

Primary B cells were acquired from C57BL/6 WT/IκBε$^{-/-}$/IκBα^{mut} female mice (9–12 weeks old), spleens were homogenized and splenocytes were stained with anti-CD43, prior to purification by negative column selection (Miltenyi Biotec, Cologne Germany) as described [14, 15]. B cell purity was assessed by flow cytometry staining for anti-B220. Mice were maintained in environmental control facilities at the University of California, Los Angeles.

Cell culture

DLBCL cell lines were obtained from the Deutsche Sammlung von Mikroorganismen und Zellkulturen (DSMZ, Braunschweig, Germany) and maintained in RPMI-1640 medium (Sigma) supplemented with 10–20% fetal bovine serum (FBS, Sigma), 1% penicillin-streptomycin (Sigma), and 1% L-glutamine (Sigma). Cells were kept at 37 °C in 5% CO_2 conditions and routinely tested for mycoplasma contamination. NIH3T3 cells transfected to stably express human CD40 (hCD40L-3T3) were obtained from Prof Chris Pepper (Brighton and Sussex Medical School, UK) and cultured in RPMI-1640 supplemented with 10% FBS, 1% penicillin-streptomycin, and 1% L-glutamine. CD40L expression was maintained through puromycin (1 μg/mL) selection.

Co-culture

To model tumor microenvironment–induced NF-κB activation, DLBCL cells were co-cultured with hCD40L-3T3 fibroblasts. Fibroblasts were seeded at 1.7×10^4 cells per well in flat-bottom 96-well tissue culture plates in 100 μL of complete media and allowed to adhere overnight. On the following day, DLBCL cells were seeded directly onto the fibroblast monolayer at 1×10^5 cells per well in 90 μL of complete media. Drug dilutions were prepared in complete media to achieve final concentrations ranging from 0.0001 μM to 100 μM. Each well received 10 μL of the appropriate drug dilution or the vehicle control (DMSO). Co-cultures were incubated for 24 h under standard conditions (37 °C, 5% CO_2).

Drug treatments

1×10^5 DLBCL cells were plated per well in 96-well plates and treated with drugs for 24 h at 37 °C in 5% CO_2. Drugs used: Amgen16-NIK inhibitor (Merck, UK), Ibrutinib-BTK inhibitor (Cambridge Biosciences, UK), AZD5991-MCL1 inhibitor (SelleckChem, USA), CW15337-NIK inhibitor, ABT199 (venetoclax)-BCL2 inhibitor (SelleckChem, USA), and A1331852-BCLXL inhibitor (SelleckChem, USA). Amgen16 was used at concentrations of 1.25–100 μM, Ibrutinib at 0.0001–100 μM, AZD5991 at 0.0001–100 μM, CW15337 at 0.0001–100 μM, ABT199 at 0.0001–100 μM, and A1331852 at 0.0001–100 μM. Re-sensitization treatments included ABT199 (0.0001–100 μM) with or without Amgen16 (50 μM) for 24 h, or with or without CW15337 (0.1 μM) for 24 h. A1331852 (0.001-100 μM) with or without Amgen16 (50 μM) for 24 h, with or without Ibrutinib (0.1 μM) for 24 h, or with or without AZD5991 (0.01 μM) for 24 h. Viability was assessed by Annexin V staining and flow cytometry.

Apoptosis assays

For viability assays performed in monoculture, DLBCL cells were seeded at 1×10^5 cells per well in U-bottom 96-well plates in 100 μL of complete media. To assess apoptosis in co-culture conditions, non-adherent DLBCL cells were collected from the top of the co-culture without disturbing the underlying fibroblast layer and transferred to U-bottom 96-well plates.

Cells were stained with Annexin V-FITC (BioLegend, UK) in 100 µL of Annexin V binding buffer (BioLegend, UK) containing 2.5 µL Annexin V per well. Samples were incubated at room temperature for 15 min in the dark and resuspended in 100 µL binding buffer for immediate acquisition on a CytoFlex LX flow cytometer (Beckman Coulter).

Flow cytometry

Apoptosis was determined by flow cytometry following Annexin V staining (BioLegend) and data was acquired on a CytoFlex LX, and data was acquired as previously described [19].

Flow cytometry was used to assess both surface and intracellular protein expression, including NF-κB subunits and anti-apoptotic BCL2-family proteins. For extracellular staining, 1 × 105 cells per well were washed and incubated in Cell Staining Buffer (BioLegend, UK) for 30 min at 4 °C. Cells were then incubated with surface antibodies in 100 µL of Cell Staining Buffer for 20 min at 4 °C in the dark. After washing, cells were fixed using Fixation/Permeabilization Solution (BD Biosciences, UK) for 20 min at 4 °C and subsequently washed three times with 1× Perm/Wash Buffer (BD Biosciences, UK). Cells were blocked in Cell Staining Buffer for 30 min at room temperature, and intracellular antibodies were added in 1× Perm/Wash Buffer for 30 min in the dark. After final washes, samples were resuspended in Cell Staining Buffer and acquired on a CytoFlex LX flow cytometer. Antibody clones, fluorophores, and suppliers are listed in Supplementary Table 1. Quantification was based on median fluorescence intensity (MFI) measurements, normalized to unstained controls.

Proteomics

Equal amounts of protein determined using BCA assay, from each sample were digested using trypsin. For tyrosine phosphoproteomics, peptides were enriched using SH2-superbinder beads as described [43], and the flow-through reconstituted in freshly prepared sample loading buffer and subjected to phosphopeptide enrichment using TiO_2 beads preconditioned with the loading buffer for 5 min. Data-independent acquisition mass spectrometry (DIA-MS) experiments were performed on a Thermo-Fisher Orbitrap Astral mass spectrometer. A DIA spectral library generated using DIA-MS2pep was utilized in DIA-NN software for protein quantification, with precursor and protein false discovery rates (FDR) set to 1%. Heatmaps were generated using R package heatmap (version 1.0.12).

Immunofluorescent microscopy

For analysis of subcellular NF-κB localisation, 2.5×10^4 DLBCL cells were seeded per well into 96-well black-walled imaging plates (PerkinElmer Ultra) in 100 µL PBS, centrifuged at 300 × *g*, and fixed in 4% paraformaldehyde for 10 min at room temperature. Cells were washed in PBS and permeabilized with 0.2% Triton X-100 for 5 min. Blocking was performed using IF Blocking Buffer (Cell Signaling Technology, UK) for 1 h at room temperature. Cells were incubated with primary antibodies targeting RelA (Cell Signaling, UK), RelB (Proteintech, UK) or cRel (Fisher, UK) (diluted in blocking buffer) for 2 h in the dark, followed by two washes in PBS-Tween 0.1%. Secondary staining was carried out with Alexa Fluor 488-conjugated secondary antibody (ThermoFisher, UK; 1:500 dilution in blocking buffer) for 1 h in the dark. Actin was stained using Rhodamine Phalloidin (ThermoFisher, UK) diluted 1:400 in PBS with 1% BSA and incubated for 1 h. Nuclear staining was performed using DAPI (ThermoFisher, UK; 1:1000 in blocking buffer) for 10 min in the dark. Following final washes, cells were stored in 200 µL PBS at 4 °C, protected from light, until imaging. Images were captured with Operetta CLS, and nuclear:cytoplasmic ratios of NF-κB proteins were analyzed with Cell Profiler (Supplementary Fig. 5). Antibody information is provided in Supplementary Table 1.

Western blotting

Whole-cell lysates were prepared in RIPA buffer (ThermoFisher, UK) supplemented with Halt protease inhibitors and EDTA. Lysates were sonicated on ice using a Bioruptor Pico (Diagenode, UK) and cleared by centrifugation. Protein concentration was quantified using the Pierce BCA Protein Assay Kit (Fisher, UK), and 40 µg of total protein per sample was denatured in LDS sample buffer with reducing agent (Invitrogen, UK), heated, and resolved by SDS-PAGE using 4–12% Bis-Tris gels (Fisher, UK). Proteins were transferred to PVDF membranes using the iBlot 2 system, and total protein was visualized using No-Stain Protein Labeling Reagent (Invitrogen, UK). Blots were blocked and incubated with primary antibodies against p100/p52 (Invitrogen, UK), followed by Alexa Fluor 680-conjugated secondary antibody (Fisher, UK). Imaging was performed using the Odyssey Fc system (Li-Cor), and band intensities were quantified using Empiria Studio (Li-Cor). All signals were normalized to total protein. Antibody information is provided in Supplementary Table 1.

Simulations

The computational model and simulation method is described previously [40]. Basal canonical pathway activation was increasing 0–0.5%. NIK degradation was decreased using the equation *NIK deg = 1/(1 + (t/600))*. 25 individual simulations were run for each cell line with parameter sampling as described previously [40, 44]. Models were solved using the Julia DifferentialEquations.jl package [45].

Statistical analysis

All statistical analysis was performed using GraphPad Prism 10.0 (California, USA) and Julia 1.8.5.

Analysis of paired datasets was performed with paired *t*tests, whereas unpaired *t* tests and one-way ANOVA to analyze differences between groups, followed by indicated post-hoc tests. LC_{50} values were generated using a post four-parameter linear regression test. Flow cytometry data was analyzed on CytExpert Software (Beckman Coulter). $^*P < 0.5$; $^{**}P < 0.01$; $^{***}P < 0.001$; $^{****}P < 0.0001$. Sample size was determined using a power calculation in which standard deviation was established by preliminary data, and sample size chosen to enable changes of 50%, to be detected with 80% power, and significance of 0.05.

RESULTS

Flow cytometry-based 'fingerprinting' predicts sensitivity to inhibitors targeting non-canonical NF-κB and BCL2

Previous work from our group introduced the use of contoured density plots standardized using z-scores to visualize NF-κB subunit abundance to establish heterogeneity in RelA abundance between ABC-DLCBL cell lines [19] (Fig. 2A). Here we apply the same visualization approach to newly generated datasets. To establish whether similar variability is present in ABC- and GC-DLBCL we measured the levels of NF-κB in two ABC- (RIVA and U2932) and two GC-DLBCL (SUDHL8 and SUDHL10) cell lines (Fig. 2B), and identified varied expression of both RelA and RelB, which did not align with Cell Of Origin (COO) classification (Fig. 2B). While there was no variability in RelB between ABC cell lines (RIVA and U2932, Fig. 2C), as reported previously [19], GC-DLBCL cell line SUDHL10 was found to have significantly higher RelB (Fig. 2B, C) and a higher ratio of RelB to RelA (Fig. 2B). Given the elevated RelB expression observed in SUDHL10, we hypothesized that this cell line may be dependent on non-canonical NF-κB signaling. The activity of non-canonical NF-κB signaling is driven by NF-κB-inducing kinase (NIK) [12]. We found NIK-inhibitor Amgen16 was significantly more effective at killing SUDHL10 cells than cell lines with lower levels of RelB (Fig. 2D, E, $p < 0.01$) [46].

We next sought to establish whether a similar approach could enable predictable targeting of BCL2-family proteins. We identified two lines with low BCL2 (SUDHL8, and SUDHL10, Fig. 2F), and two lines with significantly higher BCL2 (U2932, and RIVA, Fig. 2G, $p < 0.0001$). We measured the viability of four DLBCL cell lines in response to ABT199 with doses ranging from 0.1 nM to 100 µM. While it is known that BH3-mimetics lose specificity at doses >10 µM, we found that ABT199 had significantly higher efficacy in cell lines with high BCL2 (Fig. 2H, I, $p < 0.01$), in agreement with clinical observations [31]. Previous BH3-profiling had suggested a complete block of apoptosis in SUDHL10 cells due to loss of effector proteins (Bak/Bax) [36]; however, multiple recent studies have found substantial Bax expression in SUDHL10 cells, and implicated low BCL2 expression in resistance to venetoclax in SUDHL10 cells [34, 47]. NF-κB profiling (Fig. 2B) revealed a vulnerability to NIK inhibition (Fig. 2D, E), indicating the potential for combined NF-κB and BCL2 "fingerprinting" to inform the rational assignment of therapeutic agents targeting multiple pathways in DLBCL.

BCL2 family protein heterogeneity confers heterogenous responses to ABT199 within a biclonal DLBCL cell line

The U2932 cell line harbors two phenotypically and genetically distinct subclones. The subclone R1 is CD20, CD38 high, while the

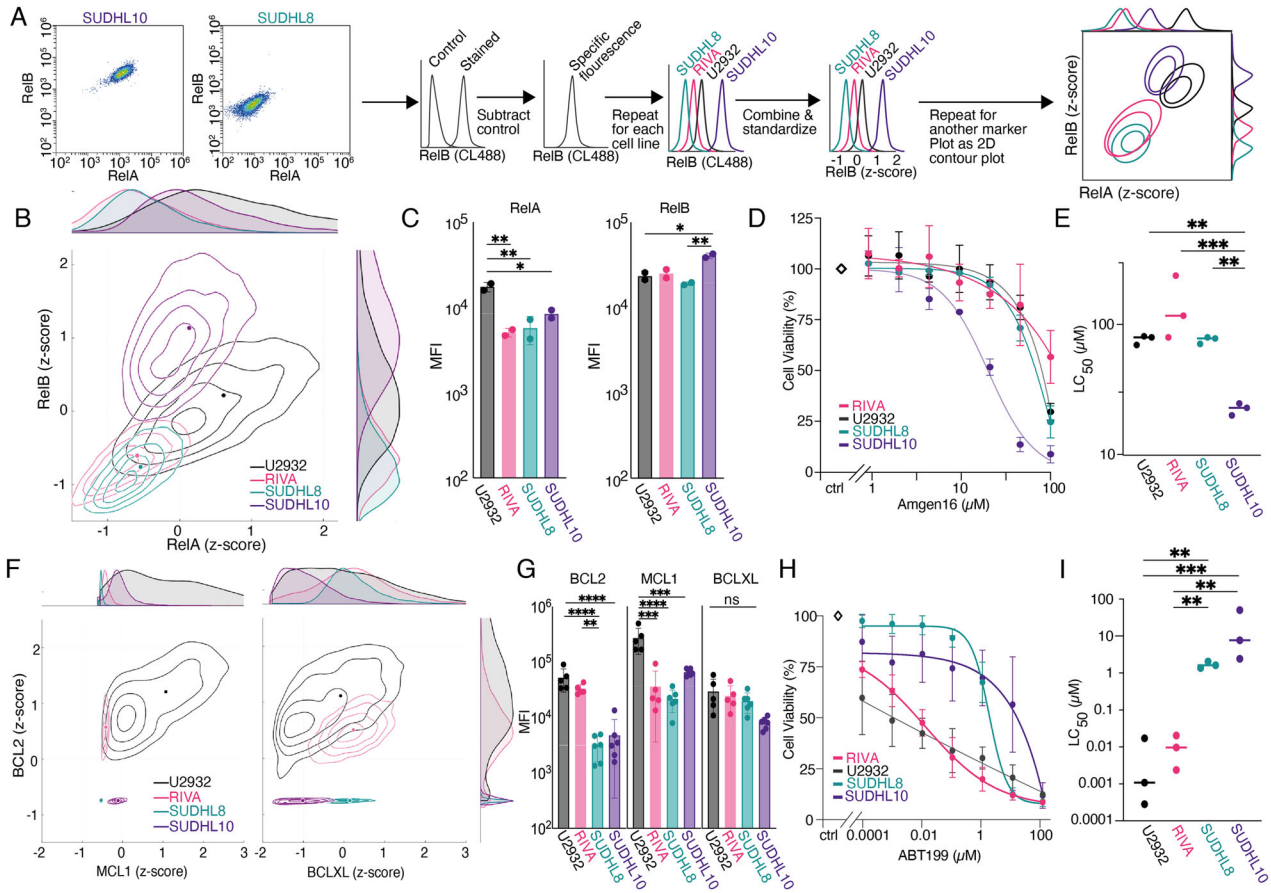

Fig. 2 NF-κB and BCL2 'fingerprinting' predicts sensitivities to inhibition of non-canonical NF-κB and BCL2 in Diffuse Large B cell Lymphoma (DLBCL). A Representative dot plots of RelA and RelB Median Fluorescence Intensity (MFI) values for the DLBCL cell lines SUDHL8, SUDHL10, U2932, and RIVA. Workflow pipeline for the productions of NF-κB fingerprints. **B** Relative RelA and RelB expression levels measured with flow cytometry, in the cell lines RIVA, U2932, SUDHL8 and SUDHL10 as fingerprints, with dots representing the median in a single experiment, also shown as probability density curves (right and top). **C** Bar graphs of RelA and RelB median fluorescence intensity (MFI) values as mean ± standard deviation of two independent experiments. (*$P < 0.05$, (**$P < 0.01$; one-way ANOVA with Tukey's comparisons test). **D** Cell viability in response to 0.125-100μM of Amgen16 in the indicated DLBCL cell lines post a 24-h treatment, error bars representing the mean ± standard deviation of three independent experiments, normalized to the untreated control. **E** LC_{50} values for the indicated cell lines in response to Amgen16 with mean indicated, three independent experiments *(**$P < 0.01$, ***$P < 0.001$ unpaired Ttest)*. **F** Relative MCL1, and BCL2, and BCLXL expression levels measured with flow cytometry, in the cell lines RIVA, U2932, SUDHL8, and SUDHL10 as fingerprints, with dots representing the median in a single experiment, also shown as probability density curves (right and top). **G** Bar graphs of MCL1, and BCL2, and BCLXL median fluorescence intensity (MFI) values as mean ± standard deviation of three independent experiments. *(**$P < 0.01$, ***$P < 0.001$, ****$P < 0.0001$; one-way ANOVA with Tukey's comparisons test)*. **H** Cell viability in response to 0.0001–100 μM of ABT199 (venetoclax) in the indicated DLBCL cell lines, post a 24-h treatment, error bars representing the mean ± standard deviation of three independent experiments, normalized to the untreated control. **I** LC_{50} values for the indicated cell lines in response to ABT199 with mean indicated, of three independent experiments *(**$P < 0.01$, ***$P < 0.001$ unpaired Ttest)*.

R2 subclone is CD20, CD38 low [19, 48]. We found that the R1 subclone (Fig. 3A) was ABT199 resistant, whereas the R2 subclone was ABT199 sensitive, even at the lowest dose of ABT199 tested (0.0001μM) (Fig. 3B). While BCL2 protein abundances could not explain the different sensitivities to ABT199 (Fig. 3C), we identified significantly higher MCL1 in the R1 subclone (Fig. 3C ,$p < 0.0001$). To determine if the selective sensitivity of the R2 subclone to ABT199 would be retained when DLBCL cells are activated by their TME we employed a co-culture system of hCD40L-3T3, which multiple studies have shown mimics both cell-contact and the presence of activated T cells in the DLBCL TME [24, 33, 34, 49] (Fig. 3D). The R2 subclone became substantially more resistant in the co-culture system (Fig. 3E), significantly increasing resistance to ABT199 (Fig. 3F, $p < 0.01$). In hCD40L-3T3 co-culture, BCLXL was significantly more induced than both BCL2 ($p < 0.05$) and MCL1 ($p < 0.01$) which were either unchanged (BCL2) or moderately decreased (MCL1) (Fig. 3G). Within the U2932 cell lines we identified multiple distinct resistance mechanisms to ABT199; high MCL1 in the R1 subclone, and high BCLXL in the context of CD40L co-culture.

TME-mediated resistance to BH3-mimetics can result from induction of multiple compensatory BCL2-family proteins

Repeating analysis in the BCL2-dependent RIVA cells identified significant TME-mediated ABT199 resistance in hCD40L-3T3 co-culture (Fig. 4A, B, $p < 0.05$) and a significant increase in BCLXL (Fig. 4C, $p < 0.01$). This effect was dependent on CD40L as untransfected NIH3T3s did not upregulate BCLXL (Supplementary Figs. 1, 2, 4).

To establish whether this effect was unique to venetoclax we employed the SUDHL8 cell line, which has established sensitivity to BCLXL inhibition by the BH3- mimetic A1331852 [34]. SUDHL8 cells were significantly resistant to BCLXL inhibition in hCD40L-3T3 co-culture (Fig. 4D, E, $p < 0.001$). Significantly more MCL1 was induced than either BCLXL or BCL2 in hCD40L-3T3 co-culture (Fig. 4F, $p < 0.05$). This effect was not seen in co-culture with untransfected NIH3T3s (Supplementary Figs. 3, 4). While CD40 is known to activate

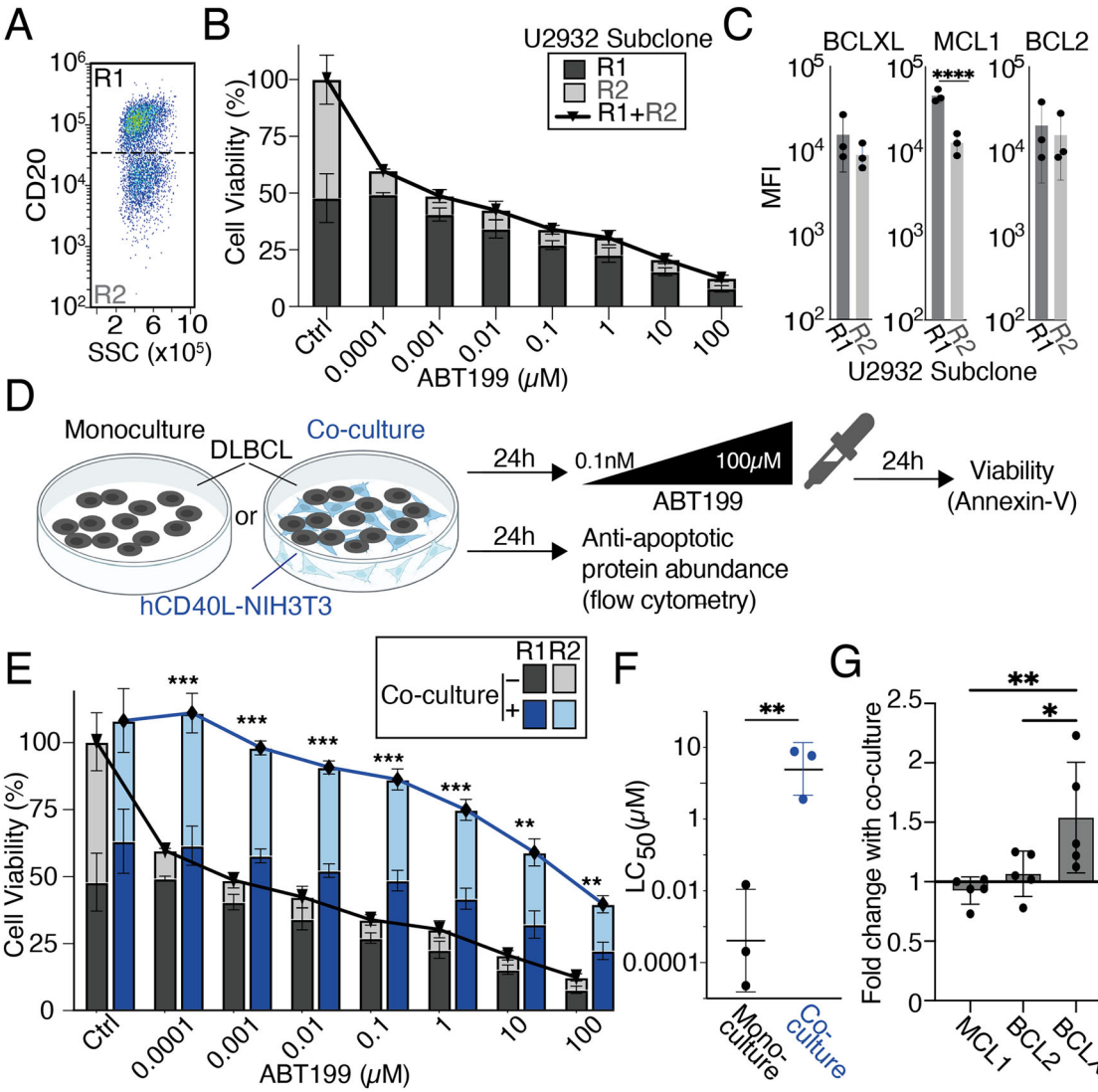

Fig. 3 Differential BCL2 family abundance in the sub-clonal cell line U2932 predicts differential responses to ABT199 (venetoclax), TME mimicking hCD40L-3T3 co-culture confers resistance to BCL2 inhibition. A Flow cytometry dot plot showing the distinct levels of CD20 Median Fluorescence Intensity (MFI) in the U2932 subclones R1 and R2. **B** Cell viability in response to 0.0001–100 μM of ABT199in the indicated U2932 subclones R1 and R2, post 24-h treatment, error bars representing the mean ± standard deviation of three independent experiments, normalized to the untreated control. **C** Bar graphs of MCL1, and BCL2, and BCLXL median fluorescence intensity (MFI) values as mean ± standard deviation of three independent experiments (*****P* < 0.0001; unpaired t-test). **D** Schematic of the co-culture system used. U2932 cells were co-cultured with hCD40L-3T3 cells prior to treatment with increasing doses of ABT199. **E** Viability of U2932 cells cultured for 24 h with or without CD40-Ligand NIH3T3 in the presence of 0.0001–100μM of ABT199. Error bars representing the mean ± standard deviation of three independent experiments, normalized to the untreated control (***P* < 0.01, ****P* < 0.001 multiple unpaired T tests using the Holm-Šídák corrections test). **F** LC50 values for the U2932 cell line in monoculture vs co-culture with hCD40L-3T3 in response to ABT199, with error bars representing the mean ± standard deviation of three independent experiments(***P* < 0.01, unpaired*T*test).**G** MCL1, BCL2, and BCLXL levels, shown as fold changes of 24-h stimulation with hCD40L-3T3 cells to unstimulated control in U2932 cells with error bars representing the mean ± standard deviation of five independent experiments (**P* < 0.05, ***P* < 0.01 one-way ANOVA with Tukey's comparisons test).

non-canonical NF-κB signaling component RelB, which has been shown to control BCLXL expression in related hematological malignancies [25], the control of MCL1 by specific NF-κB subunits is less clear, particular in the context of lymphoma (Fig. 1A).

The SUDHL8 cell line has high basal nuclear NF-κB RelA activity through elevated B cell receptor signaling

We hypothesized that the canonical RelA- or cRel-containing NF-κB dimers could be responsible for cell line-specific induction of BH3-mimetic resistance through MCL1 (Fig. 5A). Quantification of the nuclear activity of NF-κB RelA and cRel using immunofluorescence microscopy (Fig. 5B, Supplementary Fig. 5) revealed substantial cell-to-cell variability in nuclear NF-κB activity (Fig. 5C), and significantly higher nuclear RelA in the SUDHL8 cell line (Fig. 5D, bottom).

We performed global, and serine threonine proteomics in the cell line with elevated nuclear RelA (SUDHL8), a line with low nuclear RelA (U2932), and a line dependent on non-canonical signaling (SUDHL10), to test whether elevated B Cell Receptor (BCR) signaling was responsible for elevated nuclear RelA. These data show substantially elevated CD19 abundance (12.32 fold SUDHL8 compared to U2932, and 6.02 fold SUDHL8:U2932), SYK abundance (1.23 fold SUDHL8:U2932, 1.76 fold SUDHL8:U2932) and CD19 phosphorylation levels (average 55.16 fold SUDHL8:U2932, and 11.88 fold SUDHL8:SUDHL10 across 5 phosphorylation sites) in SUDHL8 compared to U2932 and

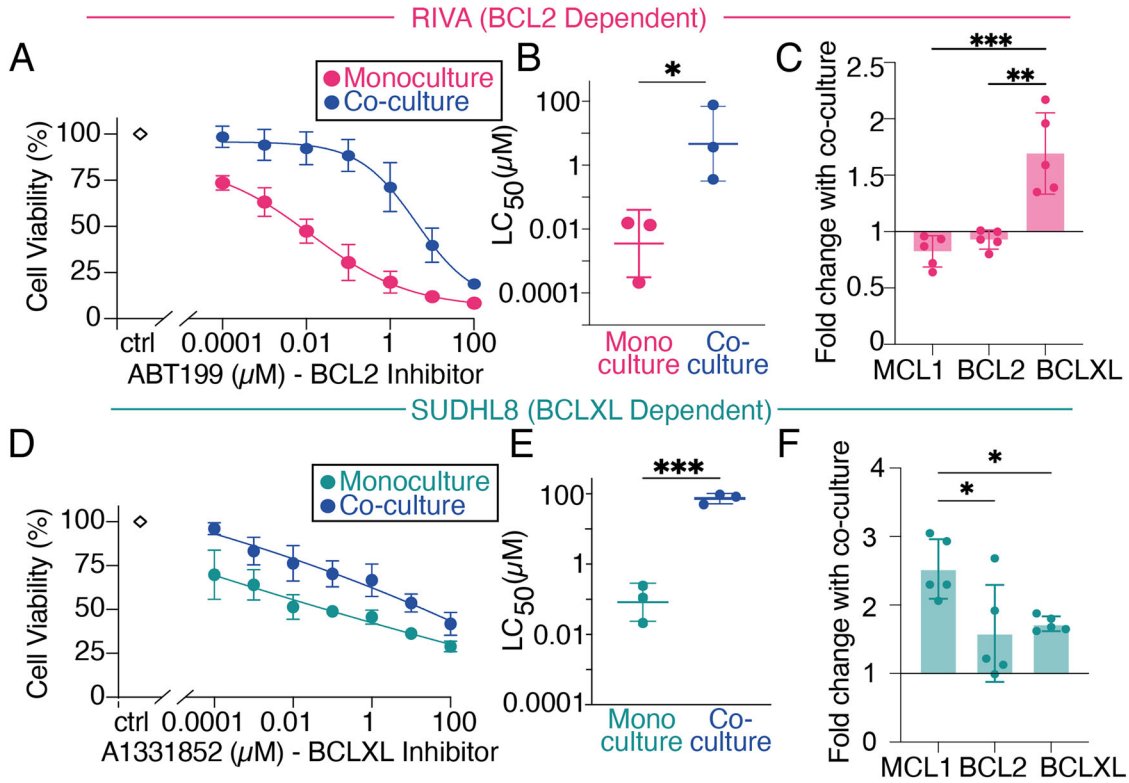

Fig. 4 Tumor microenvironment-mimicking co-culture induced resistance to BH3-mimetics in Diffuse Large B Cell Lymphoma (DLBCL) cell lines. A Viability of RIVA cells cultured for 24 h with or without hCD40L-3T3 cells in the presence of 0.0001–100μM of the BCL-2 inhibitor ABT199 (venetoclax). Error bars representing the mean ± standard deviation of three independent experiments, normalized to the untreated control. **B** LC_{50} values for RIVA in each condition with error bars representing the mean ± standard deviation of three independent experiments, normalized to the untreated control (*$P < 0.05$, unpaired *T*test). **C** MCL1, BCL2, and BCLXL levels, shown as fold changes of 24-h stimulation with hCD40L-3T3 cells to unstimulated control in RIVA with error bars representing the mean ± standard deviation of five independent experiments (**$P < 0.01$, ***$P < 0.001$ one-way ANOVA with Tukey's comparisons test. **D** Viability of SUDHL8 cells cultured for 24 h with or without hCD40L-3T3 cells in the presence of 0.0001–100 μM of the BCLXL inhibitor A1331852. Error bars representing the mean ± standard deviation of three independent experiments, normalized to the untreated control. **E** LC_{50} values for SUDHL8 in each condition with error bars representing the mean ± standard deviation of three independent experiments, normalized to the untreated control (***$P < 0.001$, unpaired *T*test). **F** MCL1, BCL2, and BCLXL levels, shown as fold changes of 24-h stimulation with hCD40L-3T3 cells to unstimulated control in SUDHL8 with error bars representing the mean ± standard deviation of five independent experiments (*$P < 0.05$, one-way ANOVA with Tukey's comparisons test).

SUDHL10 (Supplementary Fig. 6A, B). BTK abundance in SUDHL8 was not elevated; however, phosphorylated Y223 in the BTK SH3 domain has recently been found to mirror catalytic activity [50]. Phosphotyrosine (pY) proteomics revealed elevated phosphorylation at BTK_Y223 in SUDHL8 cells (1.8 fold) consistent with elevated BTK activity (Supplementary Fig. 6C).

As CD40L is a selective activator of non-canonical NF-κB signaling in B cells [51], it is not clear how elevated BTK activity and RelA nuclear abundance in SUDHL8 could confer CD40-mediated induction of MCL1 (Fig. 5A). IκBα, IκBε, and p100/IκBδ are all induced by RelA activity [12], and are preferential inhibitors of distinct NF-κB subunits (Fig. 5A) [14, 15, 40]. Therefore, we hypothesized that the altered profile of NF-κB inhibitors could control distinct responses to the TME and sought to establish how this could lead to selective induction of MCL1.

Computational modeling informed by imaging experiments predicts that high basal nuclear NF-κB RelA leads to crosstalk, with CD40-mediatead induction of cRel

Employing established computational models of NF-κB signaling [19, 40], and running two simulations differing only in the degree to which basal BCR-signaling was elevated, predicted that RelA:p50 is mainly inhibited by IκBα in RIVA cells (Fig. 6A). SUDHL8 cells were predicted to have reduced inhibition of RelA and a moderate shift in inhibitor composition (away from IκBα and IκBε, Fig. 6A–left). The predicted impact of high basal canonical pathway activation on cRel:p50 was markedly different (Fig. 6A, right), shifting towards IκBδ inhibition of cRel in SUDHL8 cells, with <14% of cRel being inhibited by IκBα and -ε (Fig. 6A right).

The steady state of these simulations (Fig. 6B, t = 0) recapitulated the selectively elevated nuclear RelA, seen in immunofluorescence imaging (Fig. 5D). Simulating co-culture mediated non-canonical pathway activation revealed induction of RelB:p52, without induction of RelA:p50 (Fig. 6B, left and center). However, induction of nuclear cRel:p50 was predicted only in the SUDHL8 cell line (Fig. 6B, right). Cells with low basal nuclear RelA, such as RIVA cells, reliably induce p100 processing to p52, and subsequent translocation of RelB:p52 to the nucleus upon CD40L activation (Fig. 6C). Simulations predict that constitutive activation of the BCR pathway results in degradation of IκBα and IκBε, nuclear translocation of RelA:p50 and subsequent induction of p100, which forms higher inhibitory complexes termed IκBδ [13]. IκBδ has higher affinity for cRel than RelA [14], resulting in sequestration of cRel by IκBδ prior to CD40L activation (Fig. 6D, left). Upon CD40L activation p100 is processed into a self-inhibited p100:p52 dimer, which frees cRel for nuclear translocation [13, 15] (Fig. 6D, right). This crosstalk mechanism was first identified in fibroblasts [13], and shown to preferentially upregulate cRel in proliferating healthy B cells responding to BAFF [15]. This predicted crosstalk from non-canonical signaling to NF-κB cRel has not previously been described in lymphoma or linked to

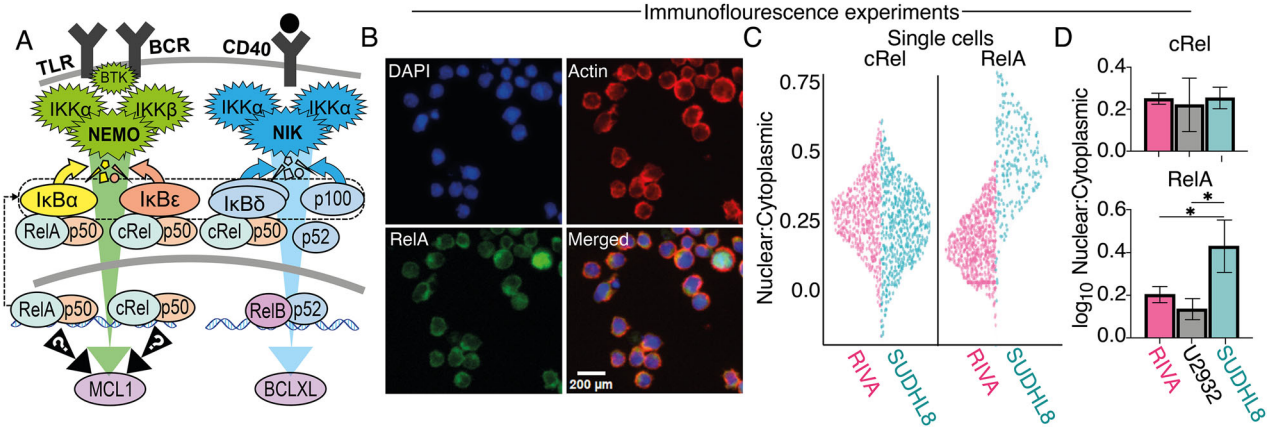

Fig. 5 Immunofluorescence microscopy reveals differential NF-κB basal RelA activity in Diffuse Large B-cell Lymphoma (DLBCL) cell lines. **A** Schematic of the canonical and non-canonical NF-κB signaling pathway illustrating how non-canonical NF-κB activation results in the induction of BCLXL and how elevated basal canonical signaling induces multiple negative regulators of NF-κB which may contribute to cell line specific induction of MCL1. **B** Representative immunofluorescence microscopy following staining in RIVA cells for RelA (NF-κB), DAPI (nucleus), actin (cytoplasm), to measure nuclear and cytoplasmic subcellular localization. **C** Quantification immunofluorescence microscopy showing nuclear to cytoplasmic ratio of cRel and RelA in single cells. Data shows a representative replicate in the indicated cell lines. Violin width indicates data density. **D** Quantification of the nuclear to cytoplasmic ratio of cRel (top) and RelA (bottom) as bar graphs with error bars of the mean ± standard deviation of three independent experiments in RIVA, U2932 and SUDHL8 (*$P < 0.05$; One-Way ANOVA).

induction of anti-apoptotic proteins, therefore we sought to validate these computational predictions.

Experimental validation of modeling predictions confirms crosstalk between CD40 and cRel confers BH3-mimetic resistance and can be overcome with BTK inhibition

Immunofluorescence imaging confirmed that hCD40L co-culture did not induce RelA (Fig. 6E, F, compare to 6B left), but did induce significantly higher levels of nuclear:cytoplasmic RelB in both the RIVA and SUDHL8 cell lines, as predicted by computational simulations (Fig. 6E, F, compared to 6B middle, $p < 0.05$). Only in SUDHL8 cells was this accompanied by significantly increased nuclear cRel, as predicted computationally (Fig. 6E, F, compared to 6B right, $p < 0.01$). hCD40L co-culture with the addition of ibrutinib (0.1 µM, targeting BTK) re-sensitized SUDHL8 cells to BCLXL inhibition, confirming BCR-pathway activation was responsible for BH3-mimetic resistance in the SUDHL8 cells (Fig. 6G, H, $p < 0.001$). Importantly, complete resensitization to the BCLXL inhibition was achieved at a dose of ibrutinib (0.1 µM) 100-fold lower than required to induce apoptosis in SUDHL8 cells when ibrutinib is used as a monotherapy (10 µM, Supplementary Fig. 7).

NF-κB cRel activity selectively induces MCL1 in B cells

We hypothesized that crosstalk-mediated induction of cRel was responsible for the induction of MCL1 (Fig. 4F). ChIP-seq data generated in a lymphoblastoid B cell line (GM12878) [52], showed promiscuous binding of all NF-κB subunits around the transcription start site (TSS) of *BCL2L1* (encoding BCLXL), and no definitive binding of NF-κB subunits at the TSS for *BCL2*. The same data revealed marginally higher levels of cRel binding than both RelB and RelA at the *MCL1* TSS (Fig. 7A). To explore whether this was unique to the lymphoblastoid cell lines we collected Model-based Analysis for ChIP-Seq 2 (MACS2) scores for NF-κB cRel, RelA and RelB within 1 kb of the MCL1 TSS across ChIP-Seq datasets reported in a ChIP-seq database (ChIP-Atlas [53], Fig. 7B) confirmed significantly higher binding of cRel than both RelA and RelB (Fig. 7B, $p < 0.0001$).

We sought an alternative method to selectively increase cRel activity in B cells. Computational modeling of NF-κB in wild type (WT) B cells, IκBε knock-out B cells, and B cells bearing an IκBα promoter mutation that lowered IκBα expression ($I\kappa B\alpha^{\kappa B/\kappa B}$), predicted that $I\kappa B\varepsilon^{-/-}$ induces cRel activity significantly more than RelA activity (Fig. 7D, $p < 0.001$), while $I\kappa B\alpha^{\kappa B/\kappa B}$ would be non-selective (Fig. 7D). This was experimentally validated using data from $I\kappa B\varepsilon^{-/-}$ mouse B cells (Alves et al. 2014, Fig. 7D, E). Primary splenic B cells from $I\kappa B\varepsilon^{-/-}$ mice (Fig. 7F, 95–99% purity, Supplementary Fig. 8) had significant selective induction of Mcl1 (Fig. 7G, $p < 0.05$), while $I\kappa B\alpha^{\kappa B/\kappa B}$ mice did not (Fig. 7G). Together, this ChIP-seq analysis, computational modeling, and validation in primary mouse models (Fig. 7D–G) implicate cRel in the upregulation of MCL1 in DLBCL.

Inhibition of the NF-κB inducing kinase (NIK) overcomes tumor microenvironment (TME)-mediated BH3-mimetic resistance in DLBCL

We sought to identify a single pharmacological intervention that could overcome the multiple methods of TME-mediated resistance to multiple BH3-mimetics identified here. In RIVA cells NIK inhibition using Amgen16 resulted in a downregulation of non-canonical pathway activity as indicated by reduced p100 to p52 processing (Fig. 8C), and selective reduction of BCLXL (Fig. 8D, $p < 0.05$). Amgen16 overcame the protective effect of the TME-mimicking co-culture and resulted in significant re-sensitization to ABT199 in RIVA cells (Fig. 8E, $p < 0.05$). To ensure this was not an off-target effect of Amgen16, we deployed an alternative NIK-inhibitor CW15337 [25], and identified a dose (0.001 µM) 1000-fold lower than the first dose that induces apoptosis in RIVA cells when used as a monotherapy (1 µM, Supplementary Fig. 9A). This low dose CW15337 completely resensitized RIVA cells to ABT199 in the context of co-culture (Fig. 8E right, $p < 0.05$, Supplementary Fig. 9B). NIK inhibition also resensitized U2932 cells to ABT199 in the context of the hCD40L-3T3 co-culture (Fig. 8F, $p < 0.05$).

We hypothesized that, in the context of hCD40L-3T3 co-culture, NIK inhibition in SUDHL8 cells would result in downregulation of both MCL1 and BCLXL, by reversing the crosstalk described in Figs. 6, 7 (Fig. 8G), which we confirmed with the addition of Amgen16 (Fig. 8H, $p < 0.05$). Treatment with Amgen16 resulted in complete re-sensitization of SUDHL8 cells to ABT199 in hCD40L-3T3 co-culture (Fig. 8I, $p < 0.001$). To confirm that re-sensitization was due to MCL1 downregulation we identified a dose of MCL1 inhibitor AZD5991 that did not induce apoptosis in SUDHL8 cells as a monotherapy (0.01 µM, Supplementary Fig. 10A), and found that this could also completely resensitize cells to BCLXL inhibition with A1331852 (Supplementary Fig. 10B, C). Importantly we could achieve an LC50 at 100-10,000 fold lower concentration of BH3-mimetics when combined with a dose of Amgen16 that induced

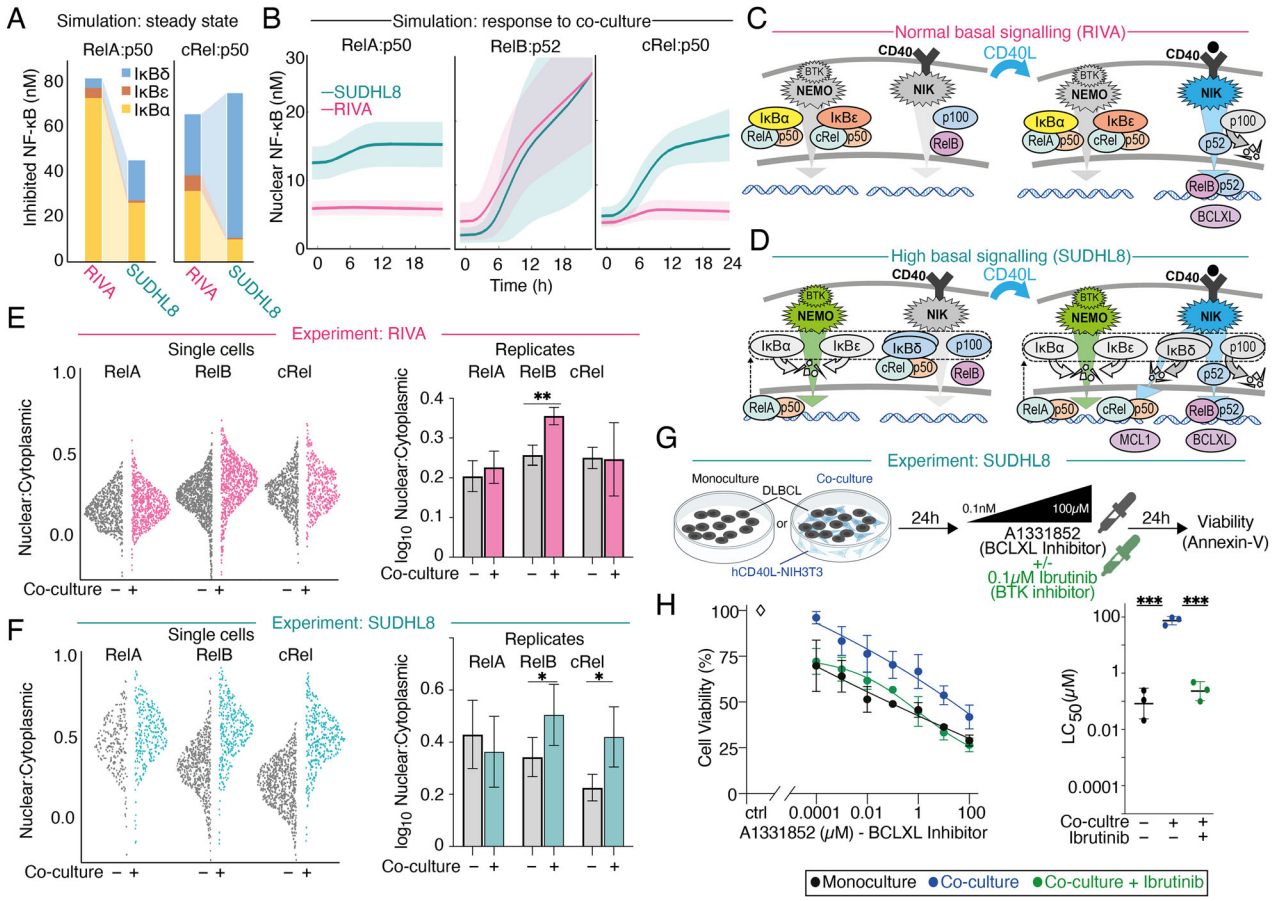

Fig. 6 Co-culture with hCD40L-3T3 cells upregulates NF-κB RelB and BCLXL in DLBCL, and selectively upregulates NF-κB cRel and MCL1 through signaling crosstalk when NF-κB RelA is chronically active. A Abundances of the heterodimers RelA:p50 (left) and cRel:p50 (right) bound to inhibiting NF-κB proteins (IκB), as simulated by computational modeling for basal canonical NF-κB activation state in RIVA, and high basal activation state in SUDHL8. See supplementary modeling description. **B** Computational modeling results showing the nuclear abundance of the indicated NF-κB dimers in a simulation with low basal nuclear RelA (RIVA, pink), and a simulation high basal nuclear RelA (SUDHL8, teal). The mean (line) and standard deviation (shaded region) of 25 cells is indicated. **C** Schematic demonstrating the mechanism by which NF-κB contributes to the induction of BCLXL in a cell line with normal basal signaling (RIVA) upon stimulation with CD40L (right). hCD40L-3T3 mediated activation of NIK results in p100 processing into p52, leading to nuclear translocation of RelB:p52 and increased expression of BCLXL. Gray = inactive pathways and low abundance proteins, color = active pathways and predominant complexes. **D** Schematic demonstrating how crosstalk emerges between CD40, NIK, cRel, and MCL1. Increase basal RelA results in increase p100, and IκBδ (left). hCD40L-3T3 mediated activation of NIK results in processing of IκBδ and release of cRel:p50, which translocates to the nucleus and potentially upregulates expression of MCL1 (right). Gray = inactive pathways and low abundance proteins, color = active pathways and predominant complexes. Quantification of immunofluorescence microscopy in RIVA (**E**) and SUDHL8 (**F**) cells showing nuclear to cytoplasmic ratio of RelA, RelB and cRel. Data post 24 h of monoculture and hCD40L-3T3co-culture is shown side by side. Single cells of a representative replicate are shown (left), with violin width indicating data density. Quantification of the nuclear to cytoplasmic ratio of RelA, RelB, and cRel is shown as bar graphs (right) with error bars displaying the mean ± standard deviation of three independent experiments (*$P < 0.05$, **$P < 0.01$; unpaired *t*test). **G** Schematic of the co-culture system used, following 24 h of treatment with 0.0001–100 μM of the BCLXL inhibitor A1331852 ± 0.1 μM of the Bruton's Kinase (BTK) inhibitor Ibrutinib. **H** Cell viability of SUDHL8 in response to 0.0001–100 μM of the BCLXL inhibitor A1331852 post a 24-h treatment in monoculture, post a 24-h hCD40L-3T3co-culture or post a 24-h hCD40L-3T3 co-culture with the addition of 0.1 μM of the BTK inhibitor, Ibrutinib. LC_{50} values for each condition is shown (right) with error bars representing the mean ± standard deviation of three independent experiments, normalized to the untreated control (***$P < 0.001$ one-way ANOVA with Tukey's comparisons test).

less than 30% cell death as a monotherapy in all cell lines (Fig. 8E,F,I, Supplementary Fig. 11).

DISCUSSION

The molecular heterogeneity that characterizes DLBCL contributes to clinical resistance and relapse [54, 55]. While there is substantial evidence that aberrant NF-κB activation within the lymph node TME, confers worse prognosis in DLBCL, the pharmacological targeting of this interaction has been challenging due to toxicities associated with targeting the canonical NF-κB pathway [56]. The present study indicates that flow cytometry fingerprinting may enable identification and assignment of NIK-inhibitors particularly in the recently identified subset of DLBCL with high RelB and poor prognosis [18]. BCL2 fingerprints confirmed that basal high basal BCL2 levels predicted sensitivity to ABT199, in accordance with results from clinical trials [57, 58]. When compared to other biochemical or functional measurements such as BH3-profiling flow cytometry-based fingerprinting enables identification of cellular sub populations within a heterogeneous tumor. We found that even within a single cell line we could identify multiple venetoclax resistance mechanisms, including inherent resistance

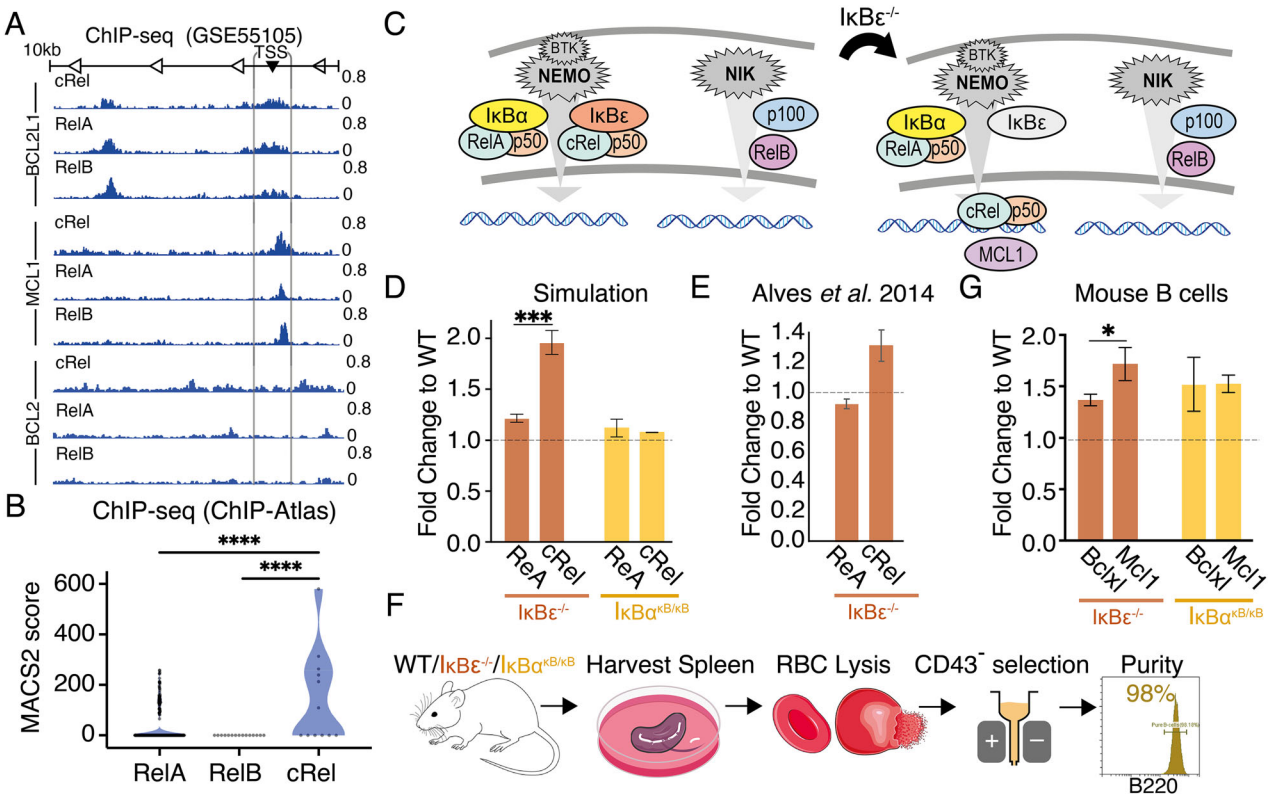

Fig. 7 IκBε knock-out mouse model reveals cRel-dependent induction of MCL1. A NF-κB ChIP-seq data from Zhao et al. 2014 [53] showing binding of the indicated NF-κB subunits around the transcription start site (TSS) of the indicated anti-apoptotic genes in lymphoblastoid B cell line. A 1 kb window around the TSS is indicated. **B** Model-based Analysis for ChIP-Seq 2 (MACS2) scores for the indicated NF-κB subunits within 1 kb of the MCL1 promoter across all ChIP-Seq datasets reported in ChIP Atlas Zou et al. 2024 [53], after outlier removal using ROUT method (q = 1%, *****P* < *0.0001*). **C** Schematic of normal basal NF-κB signaling (left), schematic of NF-κB signaling predicting the unknown effect of $I\kappa B\varepsilon^{-/-}$ on cRel and MCL-1 induction. **D** Computational modeling simulation of RelA and cRel abundance in $I\kappa B\varepsilon^{-/-}$ and $I\kappa B^{\alpha\kappa B/\kappa B}$ demonstrated as fold changes normalized to wild-type. Error bars represent the mean and ± standard deviation of 25 cells (****P* < *0.001*, unpaired *t*test). **E** RelA and cRel abundances in $I\kappa B\varepsilon^{-/-}$ and $I\kappa B\alpha^{\kappa B/\kappa B}$ cells derived from primary splenocytes, demonstrated as fold changes to wild-type, error bars representing the mean ± standard deviation. **F** Experimental pipeline showing the workflow of isolating and purifying primary B cells from wild type, $I\kappa B\varepsilon^{-/-}$ and $I\kappa B\alpha^{\kappa B/\kappa B}$ mouse genotypes. **G** Abundances of MCL1 and BCLXL acquired with flow cytometry in primary B cells isolated and purified from $I\kappa B\varepsilon^{-/-}$ (left) and $I\kappa B\alpha^{\kappa B/\kappa B}$ (right) mouse genotypes, demonstrated as fold changes normalized to wild-type. Error bars represent the mean ± standard deviation of three independent experiments (**P* < *0.05*, unpaired *t*test).

due to high MCL1, and resistance acquired in the context of a TME-mimicking co-culture through upregulation of BCLXL.

BCL2-targeting therapies create impressive responses in CLL, where the bulk of the disease is circulating in the peripheral blood, however lymph-node mediated treatment resistance has been implicated in the inability to cure CLL [59]. In DLBCL, where the bulk of the disease is supported by the lymph node TME, BCL2-targeting therapies have been far less effective. Increased non-canonical NF-κB activity, and BCLXL, may provide a rationale for the lack of efficacy of ABT199 in DLBCL. NIK inhibition was effective in all cell lines tested here: either as a monotherapy in RelB high DLBCL (Fig. 2B), to re-sensitize BCL2-sensitive DLBCL to ABT199 in the TME (Fig. 8D, E), or to re-sensitize BCLXL-sensitive DLBCL to BCLXL targeting BH3-mimetics in the TME (Fig. 8C). This finding is supported by studies in CLL [24, 25].

We discovered unexpected induction of MCL1 in cells with elevated basal NF-κB activity. Incorporating NF-κB activity information into computational models led to a prediction of signaling crosstalk between the two NF-κB pathways, which was experimentally confirmed. Our data implicate cRel as a regulator of MCL1 in DLBCL, which was previously unknown [60]. cRel-mediated gene expression has been correlated with GC-DLBCL [61], and pre-clinical MCL1 inhibitors show increased efficacy in GC-DLBCL [62]. As MCL1 inhibitors are currently reaching first-in-human studies [63], a predictive understanding of how the TME controls abundance of anti-apoptotic proteins through NF-κB will be key to successful trial design and clinical adoption. This study highlights the importance of understanding the impact of TME-mediated signaling, which may not be captured in assays performed on isolated cells or isolated mitochondria [64].

Computational simulations can: predict DLBCL responses to BH3-mimetics [39], integrate flow cytometry and mutational information to predict DLBCL signaling responses to the TME [19], and predict unexpected crosstalk between the TME and anti-apoptotic proteins. Integration of high dimensional data with computational modeling enables assignment of targeted therapies that can overcome the protective effect of the TME. While detailed molecular characterization is unlikely to be incorporated into the standard of care for all DLBCL patients, computational simulations informed by genetic profiling of diagnostic samples enable the identification of DLBCL patients that are molecularly predisposed to a poor response [41]. Such a prediction motivates further combined molecular profiling and computational modeling in order to assign efficacious targeted therapeutic approaches to the subset patients who will not respond to the standard of care.

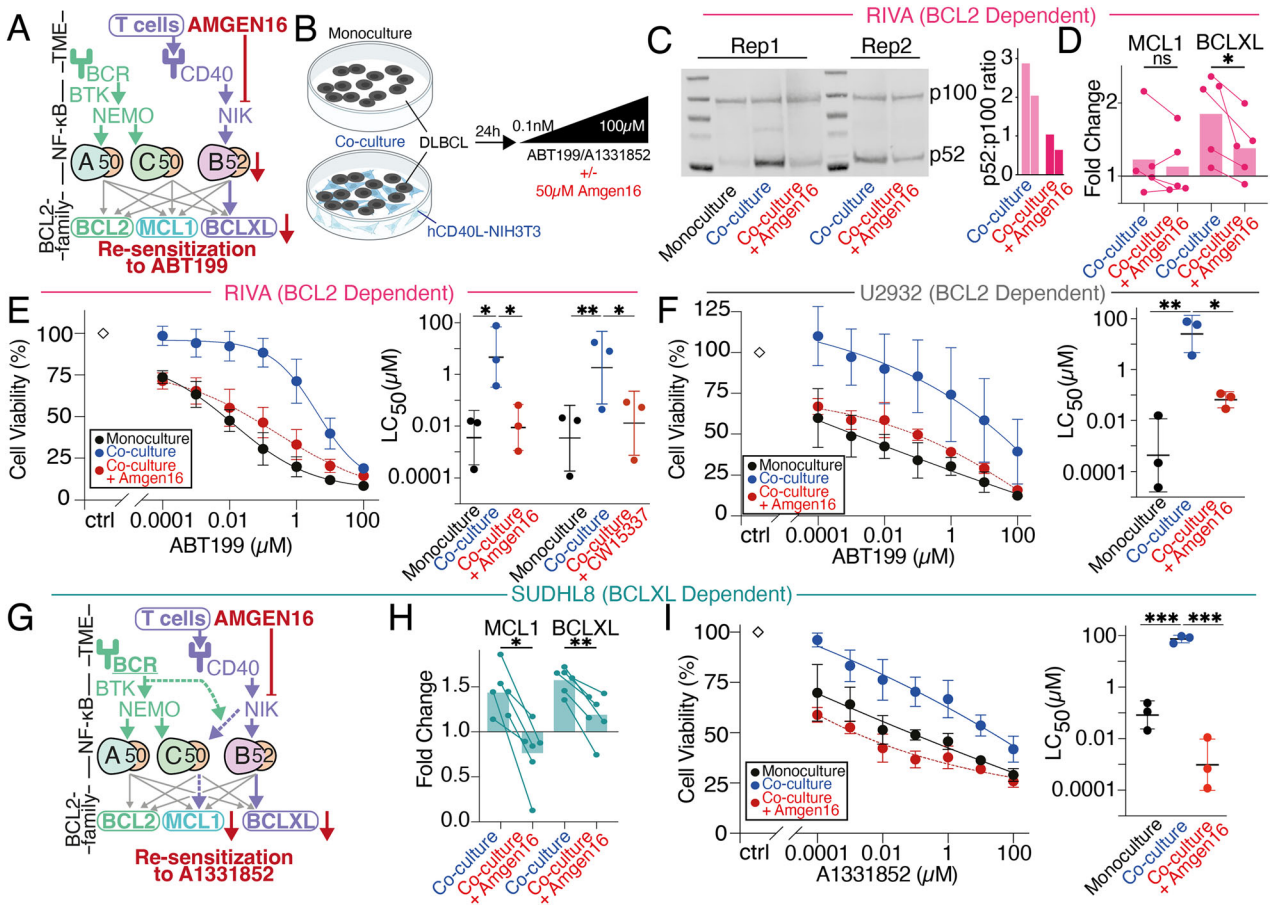

Fig. 8 Targeting the NF-κB inducing kinase (NIK) to overcome tumor microenvironment (TME) resistance in Diffuse large B cell lymphoma (DLBCL). A Overview of signaling between TME, NF-κB, and BCL2-family proteins indicating interactions revealed here with dashed lines, and NIK-inhibitor Amgen16 displayed in red. **B** Schematic of the co-culture system used, following 24 h of treatment with 0.0001–100 μM of venetoclax (ABT199) or A1331852 ± 50 μM of the NIK inhibitor Amgen16. **C** Western blot analysis of p100 and p52 levels in RIVA cells under monoculture, post a 24-h hCD40-3T3 co-culture or post a 24-h hCD40L-3T3 co-culture with the addition of 50 = μM of Amgen16. Quantification of p52:p100 ratio from western blot data, normalized to total protein across conditions. Bar graphs depict the p52:p100 ratio of two independent experiments. Uncropped blots are presented in the supplementary material. **D** Fold change to monoculture in MCL1 and BCLXL protein levels in RIVA cells under the indicated conditions. Data points represent paired measurements from individual biological replicates. Statistical analysis was performed using paired *T* tests with significance indicated as $^{*}P < 0.05$, ns = not significant. **E** Cell viability of RIVA cells in response to 0.0001–100μM of the BCL-2 inhibitor ABT199 following a 24-h treatment under three conditions: monoculture, co-culture with hCD40L-3T3 cells, and co-culture with the addition of 50 μM of the NIK inhibitor Amgen16. LC_{50} values for each condition are shown (right) with error bars representing the mean ± standard deviation of three independent experiments, normalized to the untreated control under four conditions: monoculture, co-culture with hCD40L-3T3 cells, co-culture with the addition of 50 μM of the NIK inhibitor Amgen16, and co-culture with the addition of 0.001 μM of the NIK inhibitor CW15337 ($^{*}P < 0.05$, $^{**}P < 0.01$, one-way ANOVA with Tukey's comparisons test). **F** Cell viability of U2932 cells in response to 0.0001–100 μM of ABT199 following a 24-h treatment under three conditions: monoculture, co-culture with hCD40L-3T3 cells, and co-culture with the addition of 50 μM of the NIK inhibitor Amgen16. LC_{50} values for each condition are shown (right) with error bars representing the mean ± standard deviation of three independent experiments, normalized to the untreated control ($^{*}P < 0.05$, $^{**}P < 0.01$, unpaired *T*test). **G** Schematic representation of the proposed mechanism by which NIK inhibition via Amgen16 disrupts CD40-mediated NF-κB crosstalk, thereby restoring sensitivity to A1331852 (BCLXL inhibitor) by reducing BCLXL and MCL1 levels in the presence of TME signals. **H** Fold change to monoculture in MCL1 and BCLXL protein levels in SUDHL8 cells cultured under co-culture and co-culture with Amgen16 conditions. Data points represent paired measurements from individual biological replicates. Statistical analysis was performed using paired T tests ($^{*}P < 0.05$, $^{**}P < 0.01$). **I** Cell viability of SUDHL8 cells in response to 0.0001–100μM of the BCLXL inhibitor A1331852 following a 24-h treatment under three conditions: monoculture, co-culture with hCD40L-3T3 cells, and co-culture with the addition of 50 μM of the NIK inhibitor Amgen16. LC_{50} values for each condition are shown (right) with error bars representing the mean ± standard deviation of three independent experiments, normalized to the untreated control ($^{***}P < 0.001$; one-way ANOVA with Tukey's comparisons test).

DATA AVAILABILITY

The computational code and analysis pipelines generated during and/or analyzed during the current study are available in the GitHub repository, https://github.com/SiFTW/VareliEtAl/. Any other data generated during and/or analyzed during the current study are available from the corresponding author on reasonable request.

REFERENCES

1. Davies A, Barrans S, Burton C, Mercer K, Caddy J, Chinnery F, et al. ACCEPT - combining acalabrutinib with rituximab, cyclophosphamide, doxorubicin, vincristine and prednisolone (R-CHOP) for diffuse Large B-cell Lymphoma (DLBCL): study protocol for a Phase Ib/II open-label non-randomised clinical trial. F1000Res. 2020;9:941.

2. Meng F, Zhong D, Zhang L, Shao Y, Ma Q. Efficacy and safety of rituximab combined with chemotherapy in the treatment of diffuse large B-cell lymphoma: a meta-analysis. Int J Clin Exp Med. 2015;8:17515–22.
3. Feugier P, Hoof AV, Sebban C, Solal-Celigny P, Bouabdallah R, Fermé C, et al. Long-term results of the R-CHOP study in the treatment of elderly patients with diffuse large B-cell lymphoma: a study by the Groupe d'Etude des Lymphomes de l'Adulte. J Clin Oncol. 2005;23:4117–26.
4. Tilly H, Morschhauser F, Sehn LH, Friedberg JW, Trněný M, Sharman JP, et al. Polatuzumab vedotin in previously untreated diffuse large B-cell lymphoma. N Engl J Med. 2022;386:351–63.
5. Bartlett NL, Wilson WH, Jung S-H, Hsi ED, Maurer MJ, Pederson LD, et al. Dose-adjusted EPOCH-R compared with R-CHOP as frontline therapy for diffuse large B-cell lymphoma: clinical outcomes of the phase III intergroup trial alliance/CALGB 50303. J Clin Oncol. 2019;37:1790–9.
6. Hunter E, McCord R, Ramadass AS, Green J, Westra JW, Mundt K, et al. Comparative molecular cell-of-origin classification of diffuse large B-cell lymphoma based on liquid and tissue biopsies. Transl Med Commun. 2020;5:5.
7. Swerdlow SH, Campo E, Pileri SA, Harris NL, Stein H, Siebert R, et al. The 2016 revision of the World Health Organization classification of lymphoid neoplasms. Blood. 2016;127:2375–90.
8. Vaidya R, Witzig TE. Prognostic factors for diffuse large B-cell lymphoma in the R(X)CHOP era. Ann Oncol. 2014;25:2124–33.
9. Priebe V, Sartori G, Napoli S, Chung EYL, Cascione L, Kwee I, et al. Role of ETS1 in the transcriptional network of diffuse large B cell lymphoma of the activated B cell-like type. Cancers. 2020;12:1912.
10. Pasqualucci L, Dalla-Favera R. Genetics of diffuse large B-cell lymphoma. Blood. 2018;131:2307–19.
11. Chapuy B, Stewart C, Dunford AJ, Kim J, Kamburov A, Redd RA, et al. Molecular subtypes of diffuse large B cell lymphoma are associated with distinct pathogenic mechanisms and outcomes. Nat Med. 2018;24:679–90.
12. Mitchell S, Vargas J, Hoffmann A. Signaling via the NFκB system. WIREs Syst Biol Med. 2016;8:227–41.
13. Basak S, Kim H, Kearns JD, Tergaonkar V, O'Dea E, Werner SL, et al. A fourth IκB protein within the NF-κB signaling module. Cell. 2007;128:369–81.
14. Alves BN, Tsui R, Almaden J, Shokhirev MN, Davis-Turak J, Fujimoto J, et al. IκBε is a key regulator of B cell expansion by providing negative feedback on cRel and RelA in a stimulus-specific manner. J Immunol. 2014;192:3121–32.
15. Almaden JV, Tsui R, Liu YC, Birnbaum H, Shokhirev MN, Ngo KA, et al. A pathway switch directs BAFF signaling to distinct NFκB transcription factors in maturing and proliferating B cells. Cell Rep. 2014;9:2098–111.
16. Davis RE, Brown KD, Siebenlist U, Staudt LM. Constitutive nuclear factor κB activity is required for survival of activated B cell–like diffuse large B cell lymphoma cells. J Exp Med. 2001;194:1861–74.
17. Curry CV, Ewton AA, Olsen RJ, Logan BR, Preti HA, Liu Y-C, et al. Prognostic impact of C-REL expression in diffuse large B-cell lymphoma. J Hematopathol. 2009;2:20–6.
18. Eluard B, Nuan-Aliman S, Faumont N, Collares D, Bordereaux D, Montagne A, et al. The alternative RelB NF-κB subunit is a novel critical player in diffuse large B-cell lymphoma. Blood, J Am Soc Hematol. 2022;139:384–98.
19. Jayawant E, Pack A, Clark H, Kennedy E, Ghodke A, Jones J, et al. NF-κB fingerprinting reveals heterogeneous NF-κB composition in diffuse large B-cell lymphoma. Front Oncol. 2023;13:1181660.
20. Pasqualucci L, Klein U. NF-κB mutations in germinal center B-cell lymphomas: Relation to NF-κB function in normal B cells. Biomedicines. 2022;10:2450.
21. Johnson PW, Balasubramanian S, Hodkinson B, Shreeve SM, Sun S, Srinivasan S, et al. Clinical impact of ibrutinib plus R-CHOP in untreated DLBCL coexpressing BCL2 and MYC in the phase 3 PHOENIX trial. Blood Adv. 2023;7:2008–17.
22. Younes A, Sehn LH, Johnson P, Zinzani PL, Hong X, Zhu J, et al. Randomized phase III trial of ibrutinib and rituximab plus cyclophosphamide, doxorubicin, vincristine, and prednisone in non–germinal center B-cell diffuse large B-cell lymphoma. J Clin Oncol. 2019;37:1285–95.
23. Studencka-Turski M, Maubach G, Feige MH, Naumann M. Constitutive activation of nuclear factor kappa B-inducing kinase counteracts apoptosis in cells with rearranged mixed lineage leukemia gene. Leukemia. 2018;32:2498–501.
24. Burley TA, Kennedy E, Broad G, Boyd M, Li D, Woo T, et al. Targeting the non-canonical NF-κB pathway in chronic lymphocytic leukemia and multiple myeloma. Cancers (Basel). 2022;14:1489.
25. Haselager M, Thijssen R, West C, Young L, Van Kampen R, Willmore E, et al. Regulation of Bcl-XL by non-canonical NF-κB in the context of CD40-induced drug resistance in CLL. Cell Death Differ. 2021;28:1658–68.
26. Froehlich TC, Müller-Decker K, Braun JD, Albrecht T, Schroeder A, Gülow K, et al. Combined inhibition of Bcl-2 and NFκB synergistically induces cell death in cutaneous T-cell lymphoma. Blood. 2019;134:445–55.
27. Bojarczuk K, Wienand K, Ryan JA, Chen L, Villalobos-Ortiz M, Mandato E, et al. Targeted inhibition of PI3Kα/δ is synergistic with BCL-2 blockade in genetically defined subtypes of DLBCL. Blood. 2019;133:70–80.
28. Elmore S. Apoptosis: a review of programmed cell death. Toxicol Pathol. 2007;35:495–516.
29. Cavalcante GC, Schaan AP, Cabral GF, Santana-da-Silva MN, Pinto P, Vidal AF, et al. A Cell's Fate: An Overview of the Molecular Biology and Genetics of Apoptosis. Int J Mol Sci. 2019;20:4133.
30. Monni O, Franssila K, Joensuu H, Knuutila S. BCL2 overexpression in diffuse large B-cell lymphoma. Leuk Lymphoma. 1999;34:45–52.
31. Morschhauser F, Feugier P, Flinn IW, Gasiorowski R, Greil R, Illés Á, et al. A phase 2 study of venetoclax plus R-CHOP as first-line treatment for patients with diffuse large B-cell lymphoma. Blood. 2021;137:600–9.
32. Davids MS, Roberts AW, Seymour JF, Pagel JM, Kahl BS, Wierda WG, et al. Phase I First-in-Human Study of Venetoclax in Patients With Relapsed or Refractory Non-Hodgkin Lymphoma. J Clin Oncol. 2017;35:826–33.
33. Bose P, Gandhi V, Konopleva M. Pathways and mechanisms of venetoclax resistance. Leuk lymphoma. 2017;58:2026–39.
34. Victoria MS, Anna D, Kristina H, Daniela B, Ross J, Lisa K, et al. Specific interactions of BCL-2 family proteins mediate sensitivity to BH3-mimetics in diffuse large B-cell lymphoma. Haematologica. 2020;105:2150–63.
35. Certo M, Moore VDG, Nishino M, Wei G, Korsmeyer S, Armstrong SA, et al. Mitochondria primed by death signals determine cellular addiction to anti-apoptotic BCL-2 family members. Cancer Cell. 2006;9:351–65.
36. Deng J, Carlson N, Takeyama K, Dal Cin P, Shipp M, Letai A. BH3 profiling identifies three distinct classes of apoptotic blocks to predict response to ABT-737 and conventional chemotherapeutic agents. Cancer cell. 2007;12:171–85.
37. Olesinski EA, Bhatia KS, Mahesh AN, Rosli S, Mohamed JS, Jen WY, et al. BH3 profiling identifies BCL-2 dependence in adult patients with early T-cell progenitor acute lymphoblastic leukemia. Blood Adv. 2023;7:2917–23.
38. Butterworth M, Pettitt A, Varadarajan S, Cohen GM. BH3 profiling and a toolkit of BH3-mimetic drugs predict anti-apoptotic dependence of cancer cells. Br J Cancer. 2016;114:638–41.
39. Cloete I, Smith VM, Jackson RA, Pepper A, Pepper C, Vogler M, et al. Computational modeling of DLBCL predicts response to BH3-mimetics. NPJ Syst Biol Appl. 2023;9:23.
40. Mitchell S, Tsui R, Tan ZC, Pack A, Hoffmann A. The NF-κB multidimer system model: A knowledge base to explore diverse biological contexts. Sci Signal. 2023;16:eabo2838.
41. Norris R, Jones J, Mancini E, Chevassut T, Simoes FA, Pepper C, et al. Patient-specific computational models predict prognosis in B cell lymphoma by quantifying pro-proliferative and anti-apoptotic signatures from genetic sequencing data. Blood Cancer J. 2024;14:105.
42. Ye X, Wang L, Nie M, Wang Y, Dong S, Ren W, et al. A single-cell atlas of diffuse large B cell lymphoma. Cell Rep. 2022;39:110713.
43. Bian Y, Li L, Dong M, Liu X, Kaneko T, Cheng K, et al. Ultra-deep tyrosine phosphoproteomics enabled by a phosphotyrosine superbinder. Nat Chem Biol. 2016;12:959–66.
44. Mitchell S, Roy K, Zangle TA, Hoffmann A. Nongenetic origins of cell-to-cell variability in B lymphocyte proliferation. Proc Natl Acad Sci. 2018;115:E2888–E97.
45. Rackauckas C, Nie Q. Differentialequations. jl–a performant and feature-rich ecosystem for solving differential equations in julia. J open Res Softw. 2017;5:15.
46. Demchenko YN, Brents LA, Li Z, Bergsagel LP, McGee LR, Kuehl MW. Novel inhibitors are cytotoxic for myeloma cells with NFkB inducing kinase-dependent activation of NFkB. Oncotarget. 2014;5:4554.
47. Deng W, Clipson A, Liu H, Huang Y, Dobson R, Wang M, et al. Variable responses of MYC translocation positive lymphoma cell lines to different combinations of novel agents: impact of BCL2 family protein expression. Transl Oncol. 2018;11:1147–54.
48. Quentmeier H, Amini RM, Berglund M, Dirks WG, Ehrentraut S, Geffers R, et al. U-2932: two clones in one cell line, a tool for the study of clonal evolution. Leukemia. 2013;27:1155–64.
49. Tromp JM, Tonino SH, Elias JA, Jaspers A, Luijks DM, Kater AP, et al. Dichotomy in NF-κB signaling and chemoresistance in immunoglobulin variable heavy-chain-mutated versus unmutated CLL cells upon CD40/TLR9 triggering. Oncogene. 2010;29:5071–82.
50. Estupiñán HY, Bouderlique T, He C, Berglöf A, Cappelleri A, Frengen N, et al. In BTK, phosphorylated Y223 in the SH3 domain mirrors catalytic activity, but does not influence biological function. Blood Adv. 2024;8:1981–90.
51. Homig-Holzel C, Hojer C, Rastelli J, Casola S, Strobl LJ, Müller W, et al. Constitutive CD40 signaling in B cells selectively activates the noncanonical NF-κB pathway and promotes lymphomagenesis. J Exp Med. 2008;205:1317–29.
52. Zhao B, Barrera LA, Ersing I, Willox B, Schmidt SC, Greenfeld H, et al. The NF-κB genomic landscape in lymphoblastoid B cells. Cell Rep. 2014;8:1595–606.

53. Zou Z, Ohta T, Oki S. ChIP-Atlas 3.0: a data-mining suite to explore chromosome architecture together with large-scale regulome data. Nucleic Acids Res. 2024;52:W45-53.
54. Coiffier B, Sarkozy C. Diffuse large B-cell lymphoma: R-CHOP failure-what to do?. Hematol Am Soc Hematol Educ Program. 2016;2016:366–78.
55. Raut LS, Chakrabarti PP. Management of relapsed-refractory diffuse large B cell lymphoma. South Asian J Cancer. 2014;3:66–70.
56. Prescott JA, Cook SJ. Targeting IKKβ in cancer: challenges and opportunities for the therapeutic utilisation of IKKβ inhibitors. Cells. 2018;7:115.
57. Kapoor I, Bodo J, Hill BT, Hsi ED, Almasan A. Targeting BCL-2 in B-cell malignancies and overcoming therapeutic resistance. Cell Death Dis. 2020;11:941.
58. Waclawiczek A, Leppä A-M, Renders S, Stumpf K, Reyneri C, Betz B, et al. Combinatorial BCL2 family expression in acute myeloid leukemia stem cells predicts clinical response to azacitidine/venetoclax. Cancer Discov. 2023;13:1408–27.
59. Woyach JA, Johnson AJ. Targeted therapies in CLL: mechanisms of resistance and strategies for management. Blood J Am Soc Hematol. 2015;126:471–7.
60. Liu H, Yang J, Yuan Y, Xia Z, Chen M, Xie L, et al. Regulation of Mcl-1 by constitutive activation of NF-kappaB contributes to cell viability in human esophageal squamous cell carcinoma cells. BMC Cancer. 2014;14:98.
61. Faumont N, Taoui O, Collares D, Jais J-P, Leroy K, Prévaud L, et al. C-rel is the pivotal NF-κB subunit in germinal center diffuse Large b-cell lymphoma: a LYSA study. Front Oncol. 2021;11:638897.
62. Liu T, Xu F, Thieme E, Lam V, Fan G, Nikolaenko L, et al. Pharmacologic targeting MCL1 with AZD5991 induces apoptosis and mitochondrial dysfunction in non-Hodgkin lymphoma (NHL) cells. Blood. 2020;136:33.
63. Desai P, Lonial S, Cashen A, Kamdar M, Flinn I, O'Brien S, et al. A Phase 1 First-in-Human Study of the MCL-1 Inhibitor AZD5991 in Patients with Relapsed/Refractory Hematologic Malignancies. Clinical Cancer Res. 2024;30:4844–55.
64. Moore VDG, Letai A. BH3 profiling–measuring integrated function of the mitochondrial apoptotic pathway to predict cell fate decisions. Cancer Lett. 2013;332:202–5.

ACKNOWLEDGEMENTS

We would like to thank all members of the Mitchell and Pepper labs for valuable discussions. This study was supported by Leukemia UK John Goldman Fellowship 2020/JGF/003, UKRI Future Leaders Fellowship (MR/T041889/1) and Paul Stanforth PhD Studentships (to SM, and to CP), Blood Cancer UK 23004 (to CP), MRC MR/V009095/1 (to A.P), NIH R01AI132731 and R01AI127867 (to A.H). CW15337 was a generous gift from Prof. Dr. Simon Mackay (University of Strathclyde, Glasgow, UK) and previously described [25].

AUTHOR CONTRIBUTIONS

Contribution: AV designed the research, performed experiments, analyzed data, designed figures and wrote the manuscript; HVN performed experiments, cosupervised part of the study and reviewed the manuscript; HC, EJ, EK, LS performed experiments; HZ, YL performed experiments, analyzed data, designed figures and wrote the manuscript; FS interpreted data and reviewed the manuscript; AH contributed vital new reagents, interpreted data, supervised part of the study and reviewed the manuscript; AP, CP designed the research, cosupervised the study and reviewed the manuscript; SM designed the research, supervised the study, performed experiments, analyzed data, designed figures and wrote the manuscript.

COMPETING INTERESTS

YL is a shareholder of DeepKinase Biotechnologies.

ETHICS APPROVAL AND CONSENT TO PARTICIPATE

All methods were performed in accordance with the relevant guidelines and regulations. Animal work was performed according to guidelines from the University of California, Los Angeles under approved ARC protocols (B-14-110 for breeding and R-14-126 for experiment).

ADDITIONAL INFORMATION

Supplementary information The online version contains supplementary material available at https://doi.org/10.1038/s41419-025-07942-0.

Correspondence and requests for materials should be addressed to Simon Mitchell.

Reprints and permission information is available at http://www.nature.com/reprints

Publisher's note Springer Nature remains neutral with regard to jurisdictional claims in published maps and institutional affiliations.